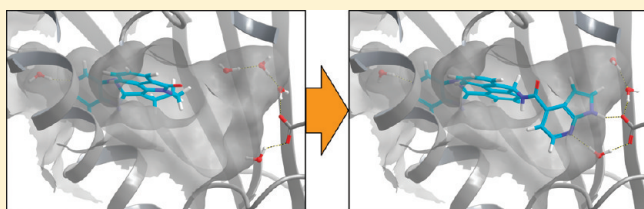


Tricyclic Series of Heat Shock Protein 90 (Hsp90) Inhibitors Part I: Discovery of Tricyclic Imidazo[4,5-*c*]pyridines as Potent Inhibitors of the Hsp90 Molecular Chaperone

François Vallée, Chantal Carrez, Fabienne Pilorge, Alain Dupuy, Annick Parent, Luc Bertin, Fabienne Thompson, Paul Ferrari, Florence Fassy, Annabelle Lamberton, Anne Thomas, Rosalia Arrebola, Stéphane Guerif, Alexandre Rohaut, Victor Certal, Jean-Marie Ruxer, Cécile Delorme, Alain Jouanen, Jacques Dumas, Claudine Grépin, Cécile Combeau, Hélène Goulaouic, Norbert Dereu, Vincent Mikol, Patrick Mailliet, and Hervé Minoux*

Sanofi-Aventis Research and Development, 13 Quai Jules Guesde, BP 14, 94400 Vitry-sur-Seine, France

ABSTRACT: A novel class of heat shock protein 90 (Hsp90) inhibitors was developed after a low throughput screen (LTS) of a focused library containing approximately 21K compounds selected by virtual screening. The initial [1-*H*-imidazo[4-5-*c*]pyridin-2-yl]-3,4-dihydro-2*H*-pyrido[2,1-*a*]isindole-6-one (**1**) compound showed moderate activity ($IC_{50} = 7.6 \mu M$ on Hsp82, the yeast homologue of Hsp90). A high-resolution X-ray structure shows that compound **1** binds into an “induced” hydrophobic pocket, 10–15 Å away from the ATP/resorcinol binding site. Iterative cycles of structure-based drug design (SBDD) and chemical synthesis led to the design and preparation of analogues with improved affinity. These optimized molecules make productive interactions within the ATP binding site as reported by other Hsp90 inhibitors. This resulted in compound **8**, which is a highly potent inhibitor in biochemical and cellular assays ($K_d = 0.35$ nM on Hsp90; $IC_{50} = 30$ nM on SKBr3 mammary carcinoma cells) and in an in vivo leukemia model.



■ INTRODUCTION

The Hsp (heat shock protein) family of molecular chaperones (Hsp27, Hsp70, Hsp90, ...) are key players in cell homeostasis, preventing improper association and assisting in the correct folding and maturation of other cellular proteins, collectively termed clients and/or substrates.¹ Heat shock protein 90 (Hsp90) is a highly conserved and a widely expressed (up to 2% of total protein content) specialized chaperone, acting on a specific subset of more than 200 client proteins, many of which are essential for constitutive cell signaling and adaptive responses to stress. Interestingly, many, even most, Hsp90 clients belong to the six hallmarks of cancer, defined by Weinberg and Hanahan,² namely transcription factors, proteins involved in angiogenesis and hypoxia, cell-cycle and signaling oncokines, tumor suppressors, and telomerase. In addition, kinases such as Bcr/abl or EGFR, including resistant mutants appearing after treatment with the first-generation kinase inhibitors Gleevec and Erlotinib, respectively, display sensitivity to Hsp90 inhibitors. Therefore, Hsp90 is recognized as a crucial facilitator of “oncogene addiction” and cancer cell survival.³

In recent years, Hsp90 has become an important target for molecular cancer therapy, having been shown to down-regulate/disrupt one or multiple oncogenic pathway(s), depending on the various tumor specificities.⁴ Following the introduction of the first Hsp90-inhibitor (17-AAG, tanespimycin) in 1999 and owing to extensive efforts in rational drug design and drug discovery,⁵

16 other Hsp90 inhibitors, all targeting the N-ter ATP pocket of Hsp90, have entered clinical trials (see Table 1).^{5c,d}

One of the most characteristic and striking features of Hsp90 protein is its extreme flexibility, which allows efficient Hsp90 chaperone cycles, in concert with cochaperones and adaptor proteins.⁶ Among documented movements that have been observed in the Hsp90 protein, conformational changes observed in the N-ter ATP site are key for the inhibition of ATP hydrolysis and client processing.

In the present paper, we report on the discovery of a new class of Hsp90 inhibitors that stabilizes Hsp90 in an inactive conformation and binds to the N-terminal ATP site in a manner as yet undescribed for other known inhibitors. In addition, we describe the further optimization of this series using structure-based drug design, which resulted in a compound with high biochemical and cellular potency as well as activity in an in vivo leukemia model.

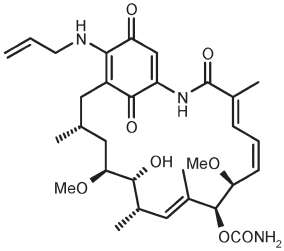
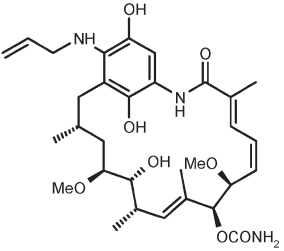
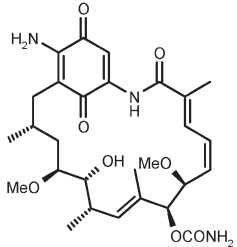
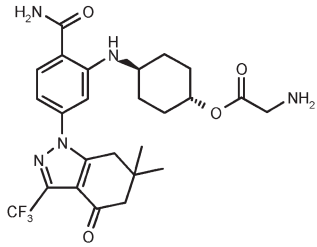
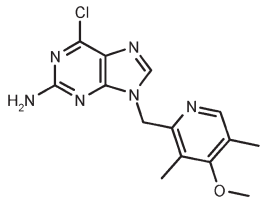
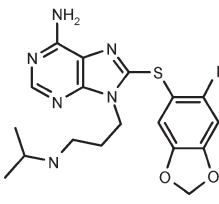
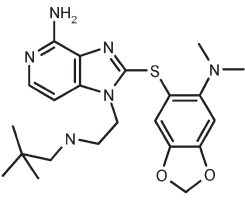
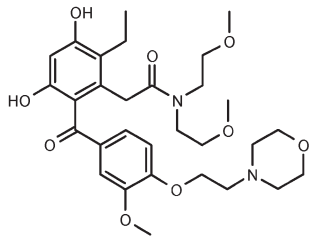
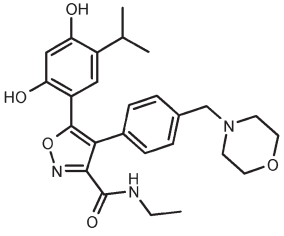
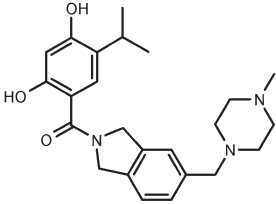
■ RESULTS AND DISCUSSION

The virtual screening of a focused library comprising 21K ATPase-oriented molecules, identified 3-(2,4-dihydroxyphenyl)-5-methyl-4-phenyl isoxazole (compound **1**, Figure 1) and 1-*H*-imidazo[4-5-*c*]pyridin-2-yl]-3,4-dihydro-2*H*-pyrido[2,1-*a*]isindole-6-one (compound **2**, Figure 1) as modest inhibitors of

Received: June 17, 2011

Published: October 05, 2011

Table 1. Hsp90 Inhibitors in Clinical Development

 <p>Tanespimycin (17-AAG)</p>	 <p>Retaspimycin (IPI-504)</p>
 <p>IPI-493</p>	 <p>SNX-5422</p>
 <p>CNF2024 / BIIB021</p>	 <p>PU-H71</p>
 <p>CUDC-305 / Debio 0932</p>	 <p>KW-2478</p>
 <p>VER-52296 / NVP-AUY922</p>	 <p>AT13387</p>
<p>Resorcinol (precise structure not reported)</p> <p>Ganetespil (STA-9090)</p>	<p>Nanoparticle albumin-bound 17-AAG</p> <p>ABI-010</p>
<p>structures not disclosed</p> <p>Other small molecules: HSP990 – BIIB028 – XL888 – DS-2248 – MPC3100</p>	

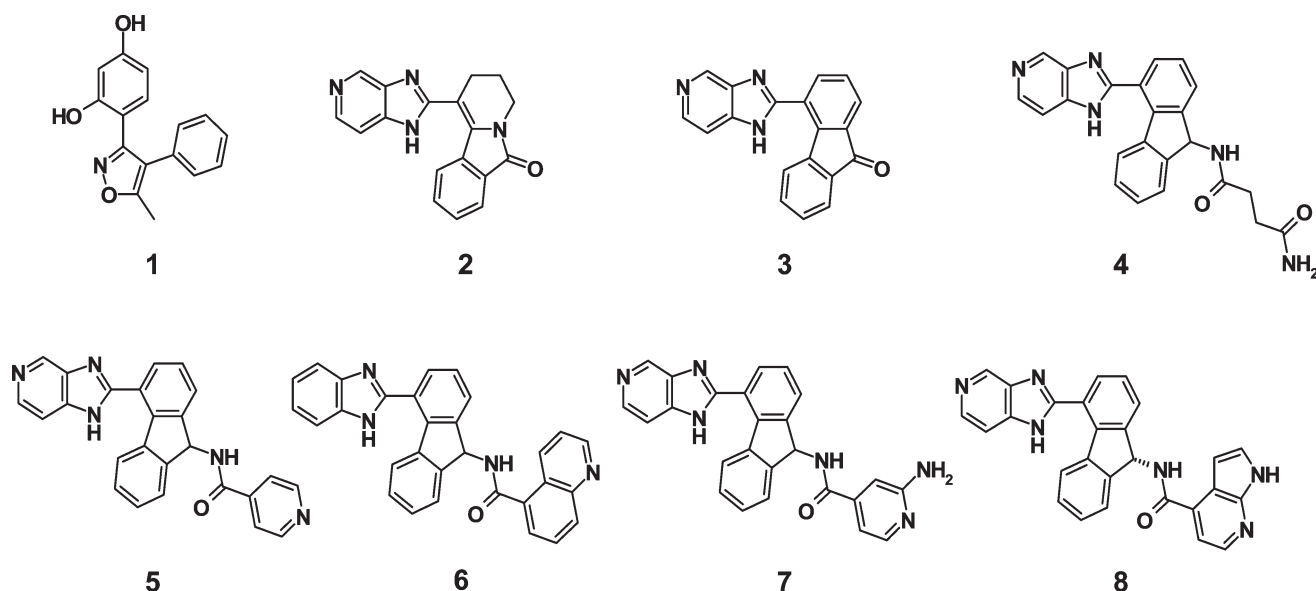


Figure 1. Chemical structures of compounds 1–8.

Table 2. Biochemical and Cellular Activities of Tricyclic Imidazo[4,5-*c*]pyridines in Comparison with Their Binding Interactions^a

compound	biochemical IC ₅₀ (μM)	cellular IC ₅₀ (μM)	binding interactions	
	yeast Hsp82 activity assay	HER2 down- regulation assay	H-bond with Asp 93	H-bond with water W1
2	7.6	>50	no	no
3	8.1	>50	no	no
4	1.1	50	yes	yes
5	0.78	1.3	no	yes
6	1.1	1.3	no	yes
7	0.61	0.9	yes	yes
8	0.49 ^a	0.03	yes	yes

^a The measure has reached the sensitivity threshold of the assay, which is 0.5 μM corresponding to half of the enzyme concentration. To determine the affinity of the compound, a *K*_d of 0.35 nM was measured on human Hsp90 in a fluorescence polarization assay.

the yeast homologue of Hsp90 and Hsp82 (IC₅₀ = 7.6 and 1.6 μM, respectively, Table 2). The scaffold of **2** was prioritized over the scaffold of **1** because of its chemical novelty. Co-crystal structures of **1** and **2** with the N-domain of Hsp90 were solved at 1.5 and 1.45 Å resolution, respectively. These compounds were shown to bind to the ATP-binding site in two different binding modes (Figure 2b,c). Hit **1** displayed the “canonical” binding mode of Hsp90 inhibitors with the presence of two critical hydrogen bonds. The first bond is observed between an hydroxyl group and Asp93; the second bond is with a bridging water molecule trapped at the bottom of the pocket. The second hydroxyl group of the resorcinol moiety makes a water-mediated contact with Asp93 Oδ2, Leu 48 O, and Ser 52 Oγ atoms. In contrast, hit **2** does not interact with Asp93 or crystallographically observed water molecules located in this region of the ATP-binding pocket. Indeed, the binding of **2** stabilizes the formation of a large hydrophobic subpocket located 10–15 Å away from Asp93.

The formation of this pocket appeared to be driven by a rearrangement of residues Ile110–Gly114 (see Figure 2a), which have previously been observed for other compounds in Hsp90.⁷ The cocrystal structure of **2** with the N-domain of Hsp90 revealed several structural features that confer tight binding in the lipophilic pocket of Hsp90 (Figure 3). First, Leu107 and its associated helix were stabilized by the imidazopyridine moiety, inducing an extended helix conformation. The conformational switch of the residues 104–111 places Leu103 and Tyr139 within hydrogen bond distance of the N/NH atoms of the imidazopyridine scaffold. This double interaction is supplemented by a water-mediated interaction between the pyridine nitrogen atom of the imidazopyridine scaffold and both main chain and side chain nitrogen atoms of residue Gln23. Second, hydrophobic residues Met98, Leu103, and Phe138, located on the other side of the pocket, make a double-stacking interaction with the pyridinoisoindolinone moiety of **2**. Finally, these structural data reveals that there is accessible space in between the carbonyl atom of the tricyclic core of **2** and Asp93. This observation suggests that a substituent, branched at the carbonyl position of **2** able to make additional interactions either with Asp93 or other accessible residues, should significantly improve the affinity of the molecule for Hsp90.

To guide further extension of molecule **2** toward Asp93, compounds **1** and **2** were cosoaked into Hsp90 crystals, resulting in a costructure with both molecules bound in the active site (Figure 4b). The solved structure of **1** + **2** (2.0 Å resolution) shows that the compound binding mode in the individual compound complexes were identical to those observed in the respective single structures. Furthermore, the superimposition of the structure of **1** + **2** with that of **1** and **2** indicated that compound **2** was occupying a region that was filled by the side chain Leu107 in the compound **1** complex. This observation was confirmed by simultaneous mass spectrometry experiment^{8,9} in which a mixture of Hsp90, compound **1**, and compound **2** gave rise to a predominant peak corresponding to the ternary complex (Figure 4a). Therefore we embarked in a rational approach based on linking compound **1** and **2** to design a molecule that will both occupy the inhibitor-induced pocket and interact with Asp93. Although the crystal structure of **1** + **2** suggests potential routes

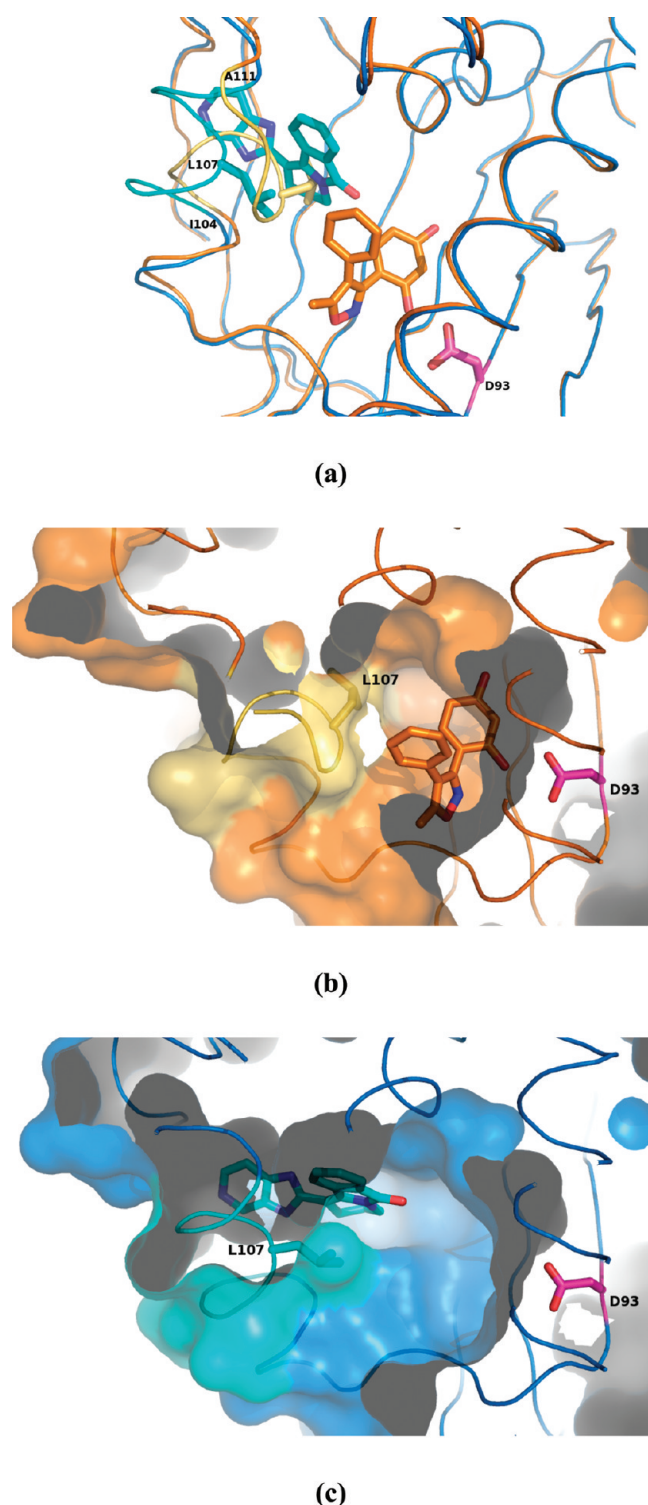


Figure 2. Comparison of Hsp90 inhibitors 1 and 2 binding modes. (a) Overlay of costructures of 1 and 2 showing the conformational flexibility of the segment 104–111 and the different binding modes of 1 and 2 in the ATP-binding pocket of Hsp90. Residue Leu107 closing the sub-pocket in the presence of 1 is shown. (b) Surface representation of the costructure of 1 showing the classical binding mode of this inhibitor located at interaction distance of residue Asp93. (c) Surface representation of the costructure of 2 set in the same orientation as (b) showing the formation of a subpocket stabilized by the presence of 2 and the movement of segment 104–111.

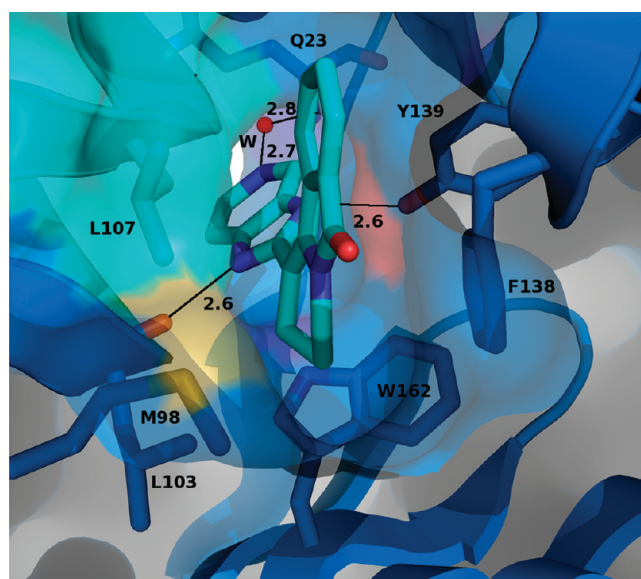


Figure 3. Sliced surface representation of the ATP-binding pocket of Hsp90 in the presence of 2. Residue Asp93 located in front of the plane of the figure is not shown (not interacting with 2). Direct and water-mediated interactions between Hsp90 and 2 are indicated using black lines, with corresponding distances in Å.

to extend compound 2 toward Asp93, linking compounds 1 and 2 directly, appears synthetically challenging. In the following text, we describe the optimization of compound 2 using iterative cycles of chemical synthesis coupled with drug design and high-resolution X-ray structures of Hsp90–inhibitor complexes used as both guides and checkpoints.

A derivative of 2 was designed and prepared to rescaffold the pyridinoisindolinone into a planar polycyclic aromatic fluorene moiety considered as a more suitable starting point for further medicinal chemistry optimization. The planarity of the fluorene moiety of 3 had no impact on changing the pattern of interactions that are observed in the costructure of 2 (data not shown). This observation is coherent with the biochemical results for 2 and 3.

The next step of the chemical optimization process focused on the design of a linker emanating from the chiral center of the fluorene moiety extending toward the ATP binding region. Computational models generated a variety of chemically plausible linkers, from which an amide linker was identified as being appropriate to bridge the fluorene moiety to substituents capable of interacting with Asp93 and surrounding residues and/or structural water molecules. A first series of compounds was designed and synthesized among which the newly introduced amide bond was extended with propylamide (4), pyridine (5), and quinoline (6) substituents, respectively (Figure 1). Although the biochemical activity obtained for those three compounds is comparable (4, $IC_{50}^{HSP82} = 1.1 \mu M$; 5, $IC_{50}^{HSP82} = 0.78 \mu M$; 6, $IC_{50}^{HSP82} = 1.1 \mu M$), the three costructures exhibit significant variations of the amide-bond geometry. In the costructure of 4, the terminal nitrogen atom of the butylamine moiety makes H-bond with Asp93 O δ 1 atom, while its terminal oxygen atom forms a water-mediated interaction with Asp93 O δ 2, Thr184 O γ , and Gly97 N atoms. This amide substituent provided the desired pattern of interaction with residue Asp93 and water molecule W1 (see Figure 5) but is probably too flexible to significantly improve inhibition potency compared to compound 3 (entropy cost).

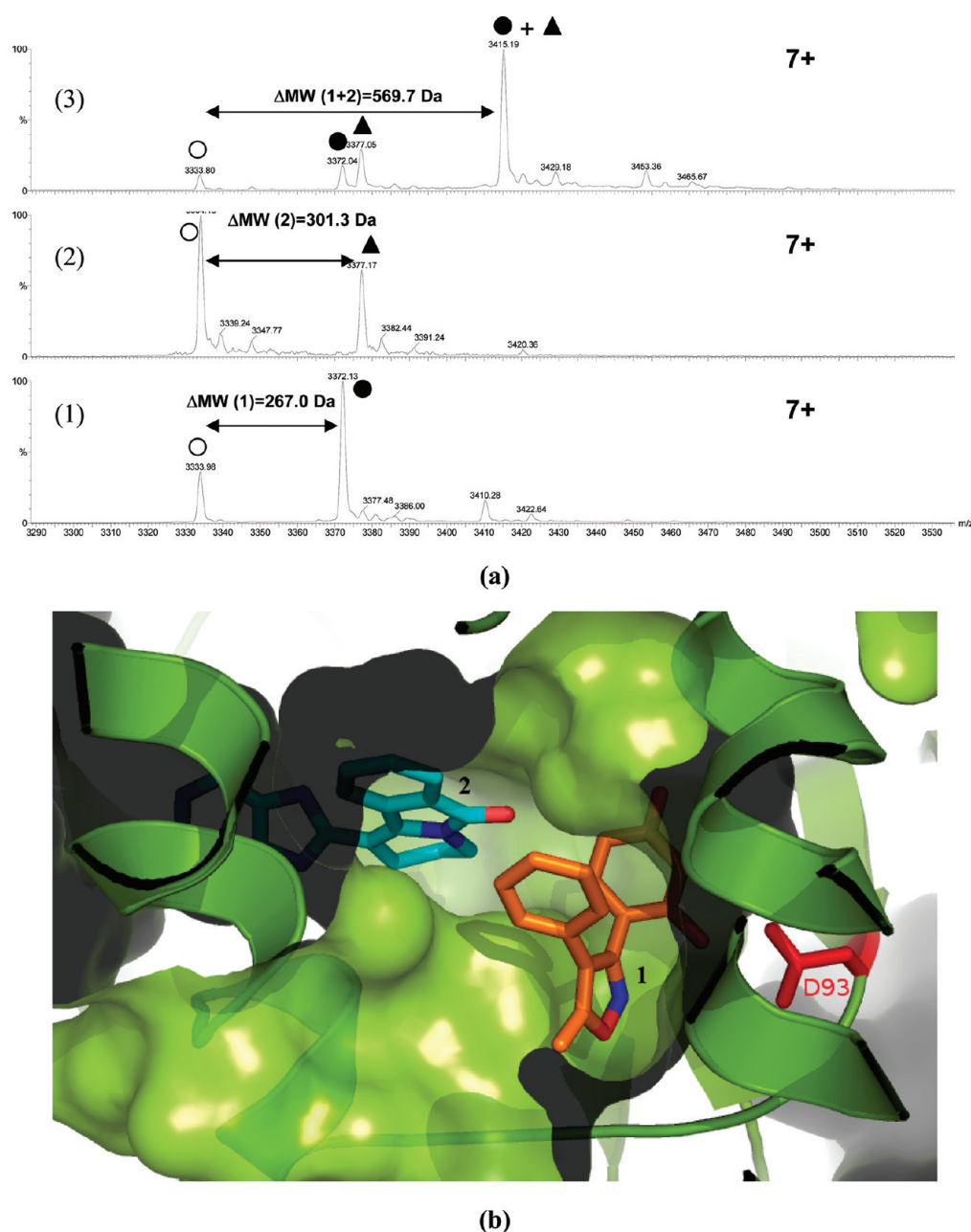


Figure 4. Ternary complex between Hsp90, 1, and 2. (a) Nanoflow electrospray mass spectra of Hsp90–inhibitors complexes: enlarged mass spectra correspond to the +7 charge state of monomeric Hsp90. (1) Hsp90–compound 1 (●) and apo Hsp90 residual (○), theoretical molecular weight (MW) (compound 1) = 267.1 Da; (2) Hsp90–compound 2 (▲) and apo Hsp90 residual (○), theoretical MW (compound 2) = 302.1 Da; (3) Hsp90–compound 1–compound 2 ternary complex (● + ▲), theoretical MW (compound 1 + compound 2) = 569.2 Da. $V_c = 35$ V. (b) Surface representation of the costructure of 1 + 2 in Hsp90. The surface of Hsp90 is colored in green, and compounds 1 and 2 are colored in orange and blue, respectively.

In the costructure of **5**, substituted with a more rigid and flat moiety, the position of the pyridine ring is such that its inner nitrogen atom interacts with W1, bringing one of its neighboring carbon atom within contact distance of the side chain of Asp93. The overlay of the costructures of compounds **4** and **5** showed that the bulkier pyridine moiety of compound **5** does not change the geometry of the amide bond seen in **4**. The carbonyl oxygen atom of the linker makes a water-mediated interaction with residue Asn51 in the two costructures (not shown in figure 5). The costructure of compound **6** shows that the nitrogen atom of

the quinoline moiety is similarly positioned than the nitrogen atom of the pyridine ring of **5** with respect to water molecule W1. However, the overlay of the costructure of **6** with those of **4** and **5** indicates that the amide bond geometry of **6** is constrained to accommodate the bulkier quinoline moiety in the ATP binding pocket. Although, a substantial gain of biochemical and cellular activity is observed with compounds **4**–**6** as compared to **2** (see Table 2), further optimization of the binding mode was undertaken to enhance potency, considering specifically, interactions with Asp93.

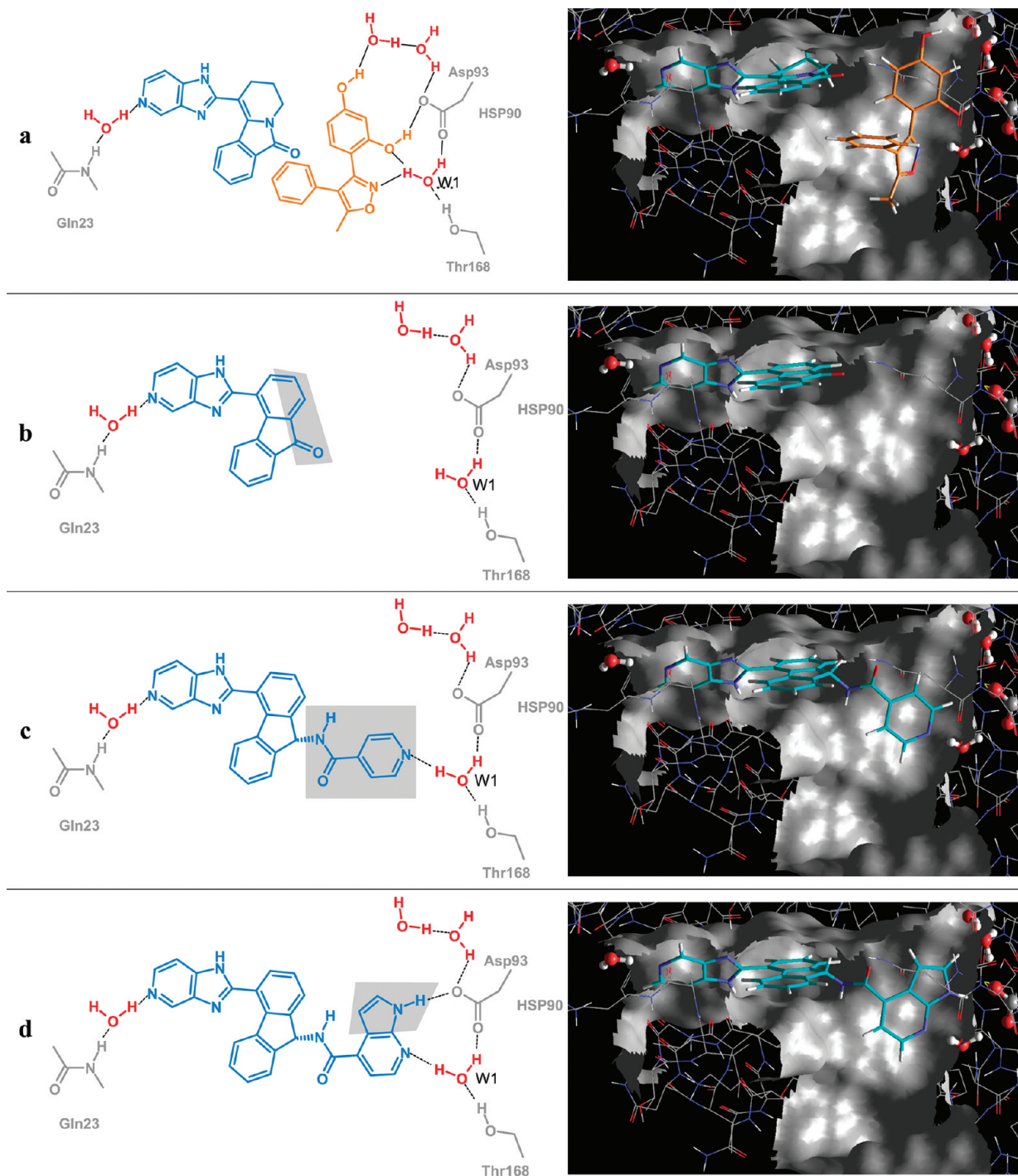


Figure 5. Key milestones of the iterative process of chemical synthesis leading to compound 8. (a) Co-structure of 1 + 2. (b) Co-structure of 3. (c) Co-structure of 5. (d) Co-structure of 8.

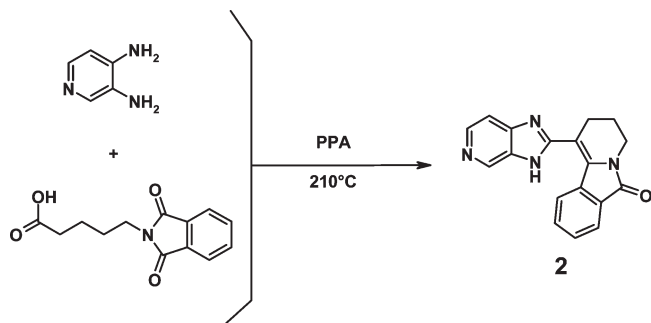
The next synthetic iteration investigated a selection of bulkier extensions to replace the pyridine moiety of compound 5. Modeling study of 7 in Hsp90 predicted an additional hydrogen bond between the amino group of the amino pyridine moiety and Asp93 O δ 2 atom. This finding was indeed confirmed in the subsequent X-ray analysis. This costructure also highlighted the presence of two alternative binding conformations of 7 in the ATP-binding pocket of Hsp90. These two conformations differed by a 180° rotation of the pyridine moiety along the amide

bond axis, resulting in alternative positioning of the extra amino group in the ATP-binding pocket. As predicted by the docking model, in one conformation, the extra amino group interacts with the Asp93 O δ 2, whereas in the second stable conformation, the amino group develops hydrogen bonds with the Gly97 O atom. This additional “alternative” hydrogen bond donor interaction between the amino group of 7 and two critical residues of the ATP-pocket of Hsp90, combined with appropriate geometry of the amide linker, was the determinant that likely resulted in

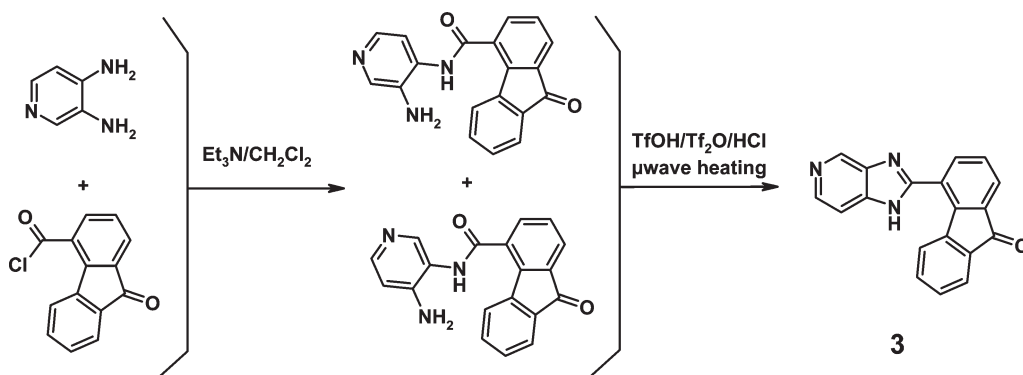
significant improvements in both biochemical and cellular activity ($IC_{50} = 0.61$ and $0.9 \mu M$, respectively), although compound 7 is properly filling the lipophilic pocket lined with lipophilic side chains of Leu48, Ile91, and Val186, and one would predict that additional hydrophobic interactions in this region might be advantageous for potency.

To achieve more efficient occupation of the ATP-binding pocket, the amino-pyridine moiety of 7 was then replaced by bulkier substituents, the intention being to make additional contacts with either Val186 or Ser52 located at the edge of this subpocket and to displace water molecules occupying this volume. A docking study of compound 7 in which the amino-pyridine was replaced by a 6-azaindole moiety predicted that the two N and NH of the azaindole would be favorably positioned to simultaneously interact with Asp93 O δ 1 (via W1) and O δ 2 atoms. This hypothesis was confirmed with the costructure of 8. Moreover, the overlay of the costructures of 4, 5, 7, and 8 indicated a shift of 8 by 0.4–0.5 Å away from Asp93 and toward Asn51. This shift is most likely observed because of the additional presence of the nitrogen atom hydrogen bond donor in 8 that directly interacts with Asp93, dictating the position of the whole inhibitor in the ATP-binding pocket of Hsp90. The overlay also showed that the five-membered ring of the azaindole moiety of 8 makes supplementary contacts with the side chains of Ser52 and Val186 and modifies the water molecule network seen in this region of the protein–inhibitor interface in the costructures 2–7. Among the three water molecules found in the costructures 2–7, the water molecule located at the vicinity of Asn51 is the only one to be displaced in the presence of 8. This displacement allows for a significant rotation of the side chain of this residue around its terminal oxygen atom, resulting in a shift of its terminal nitrogen atom of ~ 1.3 Å toward the carbonyl atom of the amide bond of 8.

Scheme 1. Synthesis of Compound 2



Scheme 2. Synthesis of Compound 3



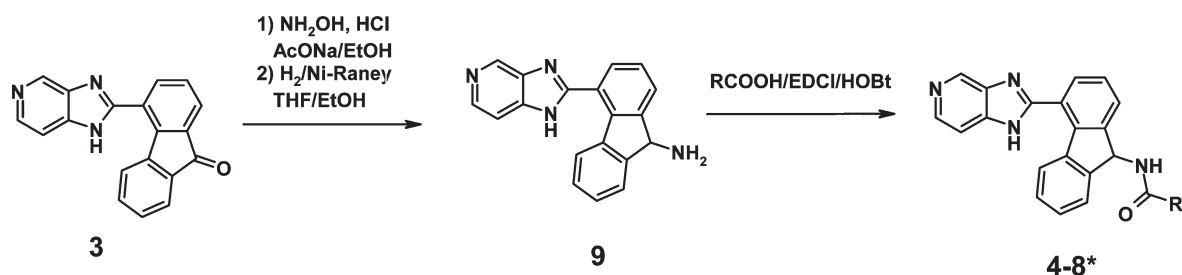
Taken together, these two structural features characterizing the costructure of 8 are most likely responsible of the newly observed interaction between the carbonyl atom of the amide bond and the side chain of Asn51.

Synthesis of Compounds 2–8. A limited number of 2,3,4,6-tetrahydro-2H-pyrido[2,1-a]isoindole ring have been reported.¹⁰ Analogous to the method described by Gourves,^{10a} pyridine-3,4-diamine and 5-(1,3-dioxo-1,3-dihydro-isoindol-2-yl) pentanoic acid were heated in polyphosphoric acid at around 210 °C, giving rise to 1-{3-H-imidazo[4,5-c]pyridin-2-yl}-3,4-dihydro-2H-pyrido[2,1-a]isoindole-6-one (2)¹¹ in a moderate yield, according to Scheme 1. Coupling of pyridine-3,4-diamine with fluoren-9-one-4-carboxylic acid chloride, followed by thermal cyclization of intermediate amides, through microwave heating in acid medium, produced a good yield of 4-(3H-imidazo[4,5-c]pyridin-2-yl)-fluoren-9-one (3),¹² according to Scheme 2. Treatment of 3 with hydroxylamine hydrochloride and sodium acetate, followed by catalytic hydrogenation of intermediate mixture of Z/E oximes, gave rise to the racemic 4-(3H-imidazo[4,5-c]pyridin-2-yl)-fluoren-9-amine (9),¹² which was further coupled with the corresponding acid to give racemates (4–8)¹² in moderate to good yields, according to Scheme 3. Chiral HPLC isolated the active dextrogyre enantiomer (8).¹² Elemental composition of compound 8 is as follows: C, 73.3%; H, 4.1%; N, 19.0%; O, 3.6%.

Comparative Bioacore Experiments with Compound (8) and 17-AAG. SPR Binding of Compound 8 and 17-AAG to Hsp90. Data represented in Figure 6 show the binding responses of compound 8 and 17-AAG to human Hsp90 that was captured on the sensor chip surface at a density of 9000 RU approximately. Under the conditions described in the Experimental Section, we found that association and dissociation rates were $k_a = 6.7 \times 10^4 M^{-1} s^{-1}$ and $k_d = 1.2 \times 10^{-4} s^{-1}$ for compound 8 and $k_a = 1.2 \times 10^4 M^{-1} s^{-1}$ and $k_d = 7.3 \times 10^{-4} s^{-1}$ for 17-AAG. This analysis produced binding constants of 1.8 and 61 nM for compound 8 and 17-AAG, respectively. Although estimated k_d for compound 8 is near the limit of Biacore S51 detection, the values are in good agreement with the k_d measured on human Hsp90 β in a fluorescence polarization assay, which were 0.35 and 7.3 nM for compound 8 and 17-AAG, respectively. In addition, the results are consistent with binding profiles previously reported for the binding of Geldanamycin to the N-terminal domain of a Met11Cys mutant Hsp90.¹³

According to the binding profile of these compounds (and several others not shown) only 20% of the immobilized protein retained the small molecule binding activity. This is lower than the homogeneously immobilized N terminal domain of Hsp90

Scheme 3. Synthesis of Compounds 4–8



* see Figure 1 for exact structures

reported by Zhou et al.¹³ Nevertheless, this immobilization procedure was preferred as no mutated protein was available to carry out this analysis.

Compound 8 Antiproliferative Data. Antiproliferative effects of compound 8 were evaluated in SKBr3 mammary carcinoma cells. A perfect correlation was observed, in SKBr3 cells, between the antiproliferative activity and the down-regulation of HER2, the major Hsp90 client in these cells, with 0.03 μ M IC₅₀ values in both cases. Antiproliferative activity of compound 8 was further addressed in a small panel of tumor cell lines, (both solid tumors and leukemia) and compared with 17-AAG, a compound already in clinical trials. As shown in Table 3, 8 and 17-AAG exhibit very similar potencies in tumor cell proliferation assays.

Compound 8 Increases Survival of B6D2F1 Mice Inoculated with P388 Murine Leukemia Cells. To assess the therapeutic potential of the tricyclic chemical series in vivo, compound 8 (6.2 mg/kg twice daily iv, four days dosing, corresponding to the highest nontoxic dose) was evaluated in B6D2F1 mice inoculated with P388 murine leukemia, in comparison with the geldanamycin derivative 17-AAG (80 mg/kg daily ip, four days dosing, corresponding to the highest tested dose owing to limited solubility). As shown in Figure 7, mice from the control group died of diffuse leukemia, as confirmed by necropsy, 9–11 days after tumor inoculation, with a median day of death (MDD) at day 10. As expected, 17-AAG treated animals showed a significant longer survival, with death occurring between day 11 and day 13. The MDD at day 13 ($p < 0.0001$ versus control group) corresponds to a 30% increase in life span (ILS). Compound 8 treated animals were characterized by an extended survival delay with death occurring between days 14 and day 18 and an MDD at day 15. The 50% ILS induced by compound 8 ($p < 0.0001$ versus control group) was significantly higher than the 30% ILS obtained for 17-AAG ($p = 0.0036$), indicating potent antitumor activity in the P388 disseminated model. These results demonstrate that compound 8 has a potentially superior in vivo antitumor activity in mice when compared to the reference Hsp90 inhibitor 17-AAG.

DISCUSSION

A new chemical series of Hsp90 inhibitor has been identified by high-throughput docking using an X-ray structure of the N-terminus domain in a closed conformation of the protein. The resulting docking pose of compound 2 was bound into the ATP binding pocket via direct H-bond interactions with water W1 (via its carbonyl moiety). The real binding mode of this compound with Hsp90 is strikingly different, as revealed by the structure of the X-ray complex described above. The discrepancy between the docking pose and the X-ray structure is explained by three different factors. First, the protein structure chosen for the

docking studies did not display the hydrophobic pocket where the compound 2 was found to bind. In addition, the structure of the protein was kept rigid during the docking (with the exception of hydrogen atoms on hydroxy and ammonium moieties). Finally, to obtain all the virtual screening results in a reasonable time frame, only one conformation of the protein was used for the docking process. The conformation of Hsp90 with the most documented inhibitor available at the time of the study (17-AAG) was selected to be used in the docking process.

The X-ray structure of Hsp90 complexed with compound 2 occupying the hydrophobic subpocket was critical in enabling us to rationalize chemical modifications for this compound and to drive subsequent optimization steps for this series. This hydrophobic subpocket has since been reported and exploited by other Hsp90 inhibitors.⁵ Our chemical optimization program has been primarily guided on targeting hot spots in the ATP-binding pocket of Hsp90 highlighted by ATP binders like compound 1. The iterative process of molecular modeling hypotheses followed by chemical synthesis, biochemical assay, and X-ray crystallography has proven to be efficient in this program to rapidly obtain the lead compound 8.

Compound 8 vs 17-AAG displays a slightly better biochemical (0.35 vs 0.54 nM) and cellular activity (HER2 down regulation assay 30 nM vs 40 nM), a lower binding constant measured by Biacore (1.8 vs 61 nM), and a longer dissociation rate ($1.2 \times 10^{-4} \text{ s}^{-1}$ vs $7.3 \times 10^{-4} \text{ s}^{-1}$). As compound 8 exhibits both a different binding mode and an improved ligand efficiency¹⁴ compared to 17-AAG (0.38 vs 0.30), we hypothesize that more effective inhibitors of Hsp90 can be identified by targeting the open conformation of Hsp90, to which compound 8 binds, as opposed to the closed form of the protein, targeted by 17-AAG. We can also speculate that the longer dissociation rate obtained for compound 8 vs 17-AAG is also linked to its particular binding mode. The longer residence time for compound 8 vs 17-AAG also translates into a better in vivo profile compared to 17-AAG as observed in the model described above, with a 20% increase in life span.

CONCLUSION

A novel class of inhibitors that potently inhibits Hsp90 has been discovered. The binding of this class of inhibitors in Hsp90 stabilizes the formation of a subpocket located ~ 10 Å from residue Asp93. Starting from a low affinity and molecular weight compound and using only a few iteration of successive cycles of computational chemistry, X-ray crystallographic analysis, and medicinal chemistry optimization, we have identified a highly potent inhibitor, compound 8, that is more active than the reference Hsp90 inhibitor in a preliminary in vivo assay. First optimized

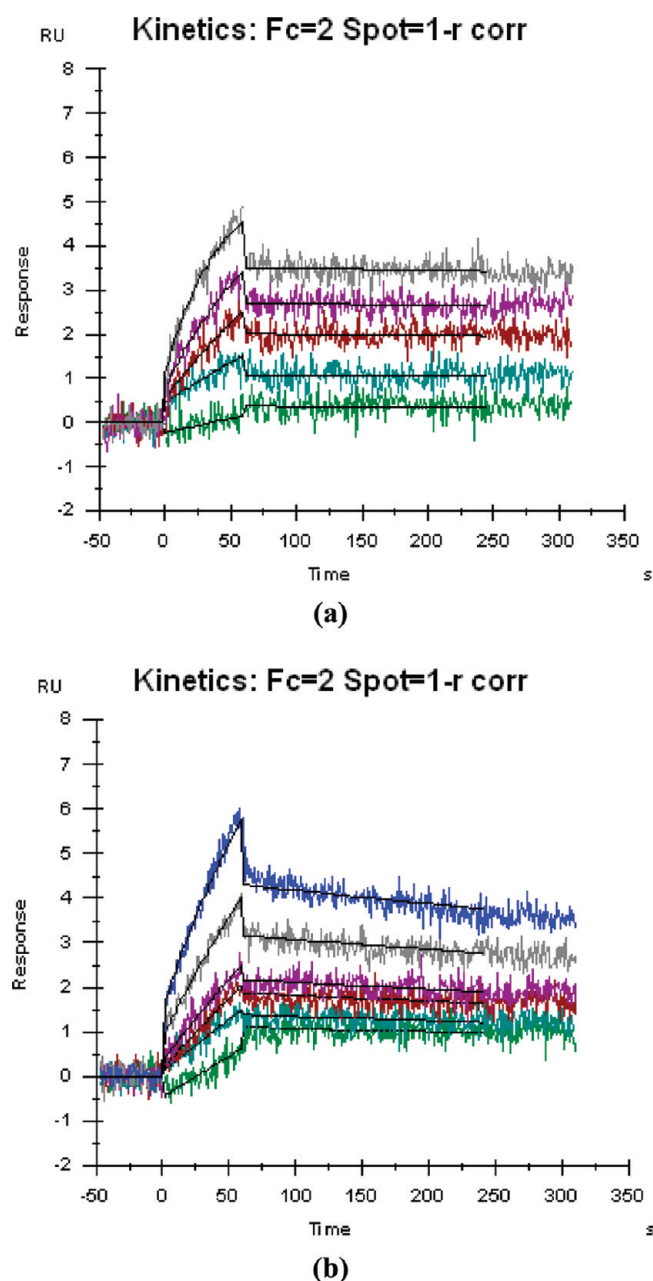


Figure 6. Kinetic analysis of compound 8 and 17-AAG binding to Hsp90. The compound 8 (a) and 17-AAG (b) were injected at concentrations of 0.023–0.375 μM (compound 8) and 0.023–0.75 μM (17-AAG) for 60 s, and dissociation was monitored for 3 min. Black lines represent the global fits of the data to a 1:1 interaction model that included a mass transport term. From the data shown here, the kinetic parameters obtained for each interaction are $k_a = 6.7 \times 10^4 \text{ M}^{-1} \text{ s}^{-1}$, $k_d = 1.2 \times 10^{-4} \text{ s}^{-1}$, $K_d = 1.8 \text{ nM}$ for compound 8, and $k_a = 1.2 \times 10^4 \text{ M}^{-1} \text{ s}^{-1}$, $k_d = 7.3 \times 10^{-4} \text{ s}^{-1}$, $K_d = 61 \text{ nM}$ for 17-AAG.

compounds of this new scaffold exhibit nanomolar antiproliferative potencies vs several cancer cell lines.

EXPERIMENTAL SECTION

Chemistry: General Procedures. Structure of compounds 1–9 have been determined by at least three different spectral methods: ^1H NMR, IR, and mass (data not shown). Purity of compounds 1–9 has

Table 3. Antiproliferative Activities of Compound 8 and 17-AAG against a Short Panel of Tumor Cell Lines

cell line	tumor type	8 IC ₅₀ μM	17-AAG IC ₅₀ μM
SKBr3	human breast	0.03	0.025
MX1	human breast	0.045	0.045
HCT116	human colon	0.03	0.145
HCT15	human colon	0.33	0.41
PC3	human prostate	0.08	0.13
H460	human lung	0.11	0.03
HT29	human lung	0.02	0.01
B16F10	murine melanoma	0.03	0.20
CEM	human ALL ^a	0.08	0.10
HL60	human AML ^b	0.04	0.06

^a ALL: acute lymphoblastic leukemia. ^b AML: acute myeloid leukemia.

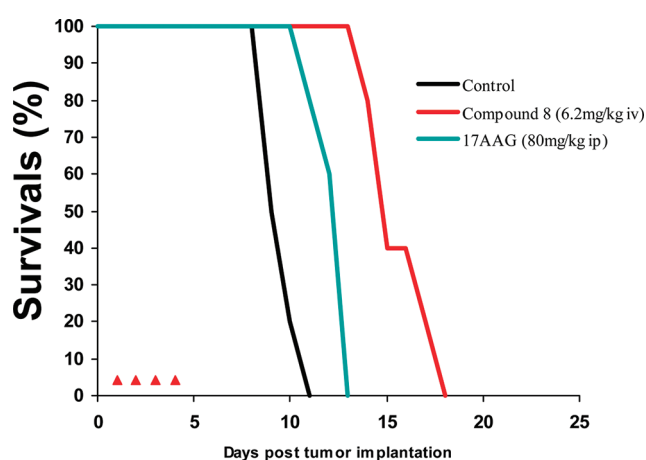


Figure 7. Kaplan–Meier survival curves of compound 8 (twice a day dosing) and 17-AAG (once a day) vs control B6D2F1 mice inoculated with 10^6 P388 leukemia cells intraperitoneally. Four days of treatment with compound 8 induced a 50% increase in life span compared to control when only a 30% increase in life span could be observed with 17-AAG for the same treatment duration.

been ascertained to be >95% by either elemental analysis or LC/MS on an AQUITY TECH C18 column eluted with water/acetonitrile gradients, containing 1% formic acid.

3-(2,4-Dihydroxyphenyl)-5-methyl-4-phenyl isoxazole (1) was prepared according to literature.¹⁵

1-{3-*H*-Imidazo[4,5-*c*]pyridin-2-yl}-3,4-dihydro-2*H*-pyrido-[2,1-*a*] isoindole-6-one (2). Four g of pyridine-3,4-diamine and 9.5 g of 5-(1,3-dioxo-1,3-dihydro-isoindol-2-yl)pentanoic acid were heated overnight at 210 °C in 45 g of polyphosphoric acid (PPA). After cooling, the mixture was diluted in water and extracted twice with ethyl acetate. The aqueous layer was kept to pH 7 and extracted six times with a 9/1 mixture of ethyl acetate and methanol. Organic layers were evaporated to dryness. Crude material was purified by flash chromatography (eluent: dichloromethane/methanol 9/1), thus yielding 1.46 g (13%) of 2, as a white powder (mp > 260 °C). ^1H NMR spectrum (400 MHz DMSO-*d*₆, δ ppm): 2.08 (m, 2H), 2.88 (t, *J* = 6.0 Hz, 2H), 3.81 (t, *J* = 6.0 Hz, 2H), 7.54 (m, 2H), 7.60 (d, *J* = 5.5 Hz, 1H), 7.78 (m, 1H), 7.95 (bm, 1H), 8.34 (d, *J* = 5.5 Hz, 1H), 8.97 (s, 1H), 12.95 (m, 1H).

4-(3*H*-Imidazo[4,5-*c*]pyridin-2-yl)-fluoren-9-one (3). Four g of pyridine-3,4-diamine, 11.5 mL triethylamine, and 10 g of fluoren-9-one-4-carboxylic acid chloride were stirred in 500 mL of methylene chloride for 4 h. The precipitate was filtered, washed with saturated sodium

hydrogenocarbonate aqueous solution, and dried at 50 °C, thus yielding 10.5 g (81%) of the equimolar mixture of both intermediate amides. The amid mixture was diluted with 20 mL of trifluoroacetic anhydride, 166 mL of trifluoroacetic acid, and 40 mL of hydrochloric acid (36%). The resulting solution was heated at 109 °C for 20 min in a 100 W microwave oven. After cooling, 500 mL of water and 500 mL of dichloromethane were added. The organic layer was discarded, and the aqueous one was kept at pH 8–9 by the addition of saturated sodium hydrogenocarbonate aqueous solution. The precipitate was filtered, washed with water, and dried at 50 °C, thus yielding 18.8 g (100%) of **3** as a pale-yellow powder (mp = 236–8 °C). ¹H NMR spectrum (400 MHz DMSO-*d*₆, δ ppm): 7.40 (td, *J* = 7.5 and 1.0 Hz, 1H), 7.49 (td, *J* = 7.5 and 1.0 Hz, 1H), 7.59 (t, *J* = 7.5 Hz, 1H), 7.62–7.73 (m, 3H), 7.82 (dd, *J* = 7.5 and 1.0 Hz, 1H), 7.90 (dd, *J* = 7.5 and 1.0 Hz, 1H), 8.41 (d, *J* = 5.5 Hz, 1H), 9.08 (s, 1H), 12.5–13.5 (m, 1H).

4-(3H-Imidazo[4,5-*c*]pyridin-2-yl)-fluorene-9(*R,S*)-amine (9). First, 14.02 g of hydroxylamine hydrochloride and 27.5 g of sodium acetate were stirred overnight with 20 g of **3** in 325 mL of ethanol. Then after dilution with 325 mL of water, the precipitate was filtered, washed with water, and dried at 50 °C, thus yielding 18 g (88%) of the equimolar mixture of *Z* and *E* 4-(3H-imidazo[4,5-*c*]pyridin-2-yl)-4-oximino-fluorene, as pale-yellow powder. ¹H NMR spectrum (400 MHz DMSO-*d*₆, δ ppm): 7.24 (m, 1H), 7.30–7.37 (m, 1H), 7.40 (m, 0.5H), 7.49 (m, 0.5H), 7.54 (t, *J* = 7.5 Hz, 0.5H), 7.49 (t, *J* = 7.5 Hz, 0.5H), 7.67–7.80 (m, 3H), 7.95 (m, 0.5H), 8.40–8.47 (m, 2H), 8.63 (m, 0.5H), 9.11 (s, 1H), 12.7–12.8 (m, 1H). A solution of 6.99 g of the above mixture of oximes in 30 mL of ethanol and 30 mL of THF was hydrogenated overnight at 60 °C under 1 bar pressure in the presence of 108 mg of Raney nickel. Catalyst was filtered off over Celite, and the solution evaporated to dryness, thus yielding 5.15 g (100%) of pure 4-(3H-imidazo[4,5-*c*]pyridin-2-yl)-fluorene-9(*R,S*)-amine (**9**), as an off-white powder. ¹H NMR spectrum (400 MHz methanol-*d*₄, δ ppm): 4.94 (s, 1H), 7.05 (d, *J* = 7.5 Hz, 1H), 7.14 (t, *J* = 7.5 Hz, 1H), 7.31 (t, *J* = 7.5 Hz, 1H), 7.51 (t, *J* = 7.5 Hz, 1H), 7.61 (d, *J* = 7.5 Hz, 1H), 7.72 (m, 2H), 7.92 (d, *J* = 7.5 Hz, 1H), 8.40 (d, *J* = 6.0 Hz, 1H), 8.99 (s, 1H).

General Method for the Preparation of Racemate Amides (4–8). One mmol of **9** and 1 mmol of corresponding carboxylic acid, which are commercially available except 1H-pyrrolo[2,3-*b*]pyridine-4-carboxylic acid prepared according to literature¹⁶ were stirred overnight at room temperature with 1 mmol of 1-(3-dimethylaminopropyl)-3-ethylcarbodiimide hydrochloride (EDCI) and 0.1 mmol of 1-hydroxybenzotriazole (HOBt) in 10 mL of DMF. After dilution with 30 mL of water, the precipitates thus obtained were filtered, washed successively with saturated aqueous sodium hydrogenocarbonate solution and water, and then dried at 50 °C. Crude racemates were further purified by flash-chromatography or HPLC/MS on silica gel. Pure eutomers, i.e. dextrogyre *R*-enantiomers, could be obtained by chiral preparative HPLC.

N-[4-(3H-Imidazo[4,5-*c*]pyridin-2-yl)-9H-fluoren-9(*R,S*)-yl]-quinoline-5-amide (4). Pale-yellow powder, mp = 254–258 °C (88%), purified by flash-chromatography on silica gel (70–230 mesh); eluent, dichloromethane/methanol (95/5). ¹H NMR spectrum (400 MHz DMSO-*d*₆, δ ppm): 6.44 (d, *J* = 8.5 Hz, 1H), 7.27 (t, *J* = 7.5 Hz, 1H), 7.39 (t, *J* = 7.5 Hz, 1H), 7.48 (m, 1H), 7.57 (t, *J* = 8.0 Hz, 1H), 7.60–7.85 (m, 5H), 7.87 (d, *J* = 7.5 Hz, 1H), 7.92 (d, *J* = 8.0 Hz, 1H), 8.14 (d, *J* = 8.5 Hz, 1H), 8.40 (d, *J* = 5.5 Hz, 1H), 8.87 (d, *J* = 8.5 Hz, 1H), 8.93–9.10 (m, 1H), 8.99 (dd, *J* = 2.0 and 4.0 Hz, 1H), 9.39 (d, *J* = 8.5 Hz, 1H), 13.3–13.5 (m, 1H).

N-[4-(3H-Imidazo[4,5-*c*]pyridin-2-yl)-9H-fluoren-9(*R,S*)-yl]-succinamide (5). White solid, mp > 260 °C (73%), isolated as its trifluoroacetate salt after purification by HPLC/MS on Symmetry C18 (5 μm) silica; eluent, gradient from 100% water (+0.07% TFA) to 100% acetonitrile (+0.07% TFA). Mass spectrum (*E*/I): *m/z* = 397 (*M*⁺).

N-[4-(3H-Imidazo[4,5-*c*]pyridin-2-yl)-9H-fluoren-9(*R,S*)-yl]-nicotinamide (6). White crystals, mp = 242 °C (46%), purified by flash-chromatography on silica gel (70–230 mesh); eluent, dichloromethane/methanol (95/5). ¹H NMR spectrum (400 MHz DMSO-*d*₆, δ ppm):

6.36 (d, *J* = 8.5 Hz, 1H), 7.26 (t, *J* = 7.5 Hz, 1H), 7.34 (t, *J* = 7.5 Hz, 1H), 7.48–7.60 (m, 3H), 7.65–7.77 (m, 3H), 7.87 (d, *J* = 6.0 Hz, 2H), 8.39 (d, *J* = 5.5 Hz, 1H), 8.75 (d, *J* = 6.0 Hz, 2H), 9.04 (s, 1H), 9.47 (d, *J* = 8.5 Hz, 1H), 13.0–14.0 (m, 1H).

2-Amino-N-[4-(3H-imidazo[4,5-*c*]pyridin-2-yl)-9H-fluoren-9(*R,S*)-yl]-nicotinamide (7). White meringue, mp = 238 °C (23%), purified by flash-chromatography on silica gel (70–230 mesh); eluent, dichloromethane/methanol (90/10). ¹H NMR spectrum (400 MHz DMSO-*d*₆, δ ppm): 6.11 (s, 2H), 6.31 (d, *J* = 8.5 Hz, 1H), 6.90–6.95 (m, 2H), 7.24 (t, *J* = 7.5 Hz, 1H), 7.33 (t, *J* = 7.5 Hz, 1H), 7.45–7.57 (m, 3H), 7.62 (m, 1H), 7.66–7.72 (m, 2H), 7.99 (d, *J* = 5.5 Hz, 1H), 8.40 (d, *J* = 5.5 Hz, 1H), 8.93–9.10 (m, 1H), 9.19 (d, *J* = 8.5 Hz, 1H), 13.2–13.5 (m, 1H).

N-[4-(3H-Imidazo[4,5-*c*]pyridin-2-yl)-9H-fluoren-9(*R,S*)-yl]-1H-pyrrolo[2,3-*b*]pyridine-4-carboxamide (rac-8). Off-white powder, mp = 236 °C (88%), purified by flash-chromatography on silica gel (70–230 mesh); eluent, dichloromethane/methanol (95/5).

N-[4-(3H-Imidazo[4,5-*c*]pyridin-2-yl)-9H-fluoren-9(*R*)-yl]-1H-pyrrolo[2,3-*b*]pyridine-4-carboxamide (8). White powder, resolved (44%) by “supercritic” HPLC on Chiralcel silica (20 μm); eluent, 100 bar CO₂/methanol/triethylamine (70/30/0.1). ¹H NMR spectrum (400 MHz DMSO-*d*₆, δ ppm): 6.42 (d, *J* = 8.5 Hz, 1H), 6.90 (m, 1H), 7.25 (t, *J* = 7.5 Hz, 1H), 7.35 (t, *J* = 7.5 Hz, 1H), 7.47 (d, *J* = 5.0 Hz, 1H), 7.50–7.57 (m, 2H), 7.60–7.72 (m, 4H), 7.79 (d, *J* = 7.5 Hz, 1H), 8.29 (d, *J* = 5.0 Hz, 1H), 8.37 (d, *J* = 5.5 Hz, 1H), 9.04 (bs, 1H), 9.28 (d, *J* = 8.5 Hz, 1H), 11.85 (bs, 1H), 13.35 (bm, 1H). α^D₂₀ = +136.5 ± 2 °C (*c* = 0.507; DMSO).

Virtual Screening. A focused screening set of molecules comprising an in-house data set of ~19K kinase-oriented compounds and a selection of ~2200 compounds made by Virtual screening was prepared. The rationale to use potential kinase inhibitor against Hsp90 being that both enzymes bind ATP and show ATPase activity. Therefore they should possess common pharmacophoric features. The selection of compounds made by Virtual Screening followed the hereafter flowchart. Starting from an in-house diverse collection of 580000 compounds, the rule of five¹⁷ and a rough pharmacophoric filter were applied. The resulting 68200 molecules which passed these filters were then docked into the binding pocket of Hsp90 using GOLD.¹⁸ During the docking process, two hydrogen-bond constraints were added, one with Asp93 and a second one with water W1. GOLD provided docking solutions for 21530 compounds. The top-ranked compounds were visually inspected, and the final selection involved clustering based on molecular similarity to expose the largest chemical diversity for the final set of 2200 compounds. Out of those 21K compounds tested in the yeast Hsp82 ATPase assay, 1084 exhibit at least 50% inhibition at 30 μM.

Structure-Based Drug Design. All X-ray structures of Hsp90 complexes were prepared by adding hydrogen and minimizing these hydrogen atoms while keeping heavy atoms frozen. Maestro by Schrödinger¹⁹ was used to visually analyze the binding pocket of Hsp90, identify area to create new interactions, and build newly modified compounds. New organic compounds were refined by running a conformational search using MacroModel with the OPLS force field²⁰, and resulting low energy conformations were visualized in the binding pocket to evaluate the new compound and identify potential steric clashes. When the resulting conformations of the organic compounds were doubtful, Conquest was used to search for analogous structures in the Cambridge Structural Database (CSD)²¹ and, if needed, structural modifications were made accordingly to the most populated geometry observed in the CSD.²²

Protein Production and Crystallography. The human Full Length Hsp90β (NP_031381) was cloned into a pAcSG2 (Baculovirus (type Pharmingen)), viral stocks produced in *Spodoptera frugiperda* (Sf9) according to the manufacturer's instructions (Invitrogen). Then high five cells were infected with recombinant viruses at a multiplicity of

infection (MOI) of 3 with the baculoviruses encoding Hsp90 at 25 °C for 72 h. Three days post infection, cells were harvested and lysed by sonification in 50 mM potassium phosphate buffer at pH 7.2 with NaCl 0.1 M. Hsp82 was produced using a protocol adapted from C. Prodromou et al.²³ Briefly, *Saccharomyces cerevisiae* strain was grown at 35 °C on synthetic medium complemented with appropriate amino acids. At the end of the exponential growing phase, temperature was increased up to 42 °C during 1 h and then the cells were harvested. Glass beads were used for yeast lyses.

S. cerevisiae Hsp82 and human Full Length Hsp90 β were purified within four chromatography steps: anion exchange chromatography (QFF, GE Healthcare), hydrophobic interaction chromatography (Phenyl HP Sepharose, GE Healthcare), ceramic hydroxyl apatite (CHT type II, BioRad), and size exclusion chromatography (Superdex 200, GE Healthcare).

A hexa-histidine tagged N-terminal fragment of Hsp90 α (18–223) (NP_005339) was cloned into a pQE30 vector and expressed in BL21 (DE3) *Escherichia coli* strain. Cells were grown in LB medium at 22 °C, and then the induction was done by using IPTG. After harvest, cells were lysed by sonification in 50 mM potassium phosphate buffer at pH 7.2 with NaCl 0.1M. The protein Hsp90 α (18–223) was captured on Ni affinity column (chelating Sepharose, GE Healthcare), followed by removal of the tag using the Tev protease. Then the protein was purified on anionic exchanger at pH 7.0 (Q-Sepharose FF, GE Healthcare) and SEC (Superdex 200, GE Healthcare). The protein was concentrated to 20 mg/mL prior to crystallization. Structures 1–8 were obtained by cocrystallization at 4 °C, for which the protein was mixed with 2 mM compound. Structure 1 + 2 was obtained by cocrystallization at 4 °C using a sequential mixture of 2 mM of 1 followed, 24 h later, by 2 mM of 2 in Hsp90. Automated crystallization setup using a Cartesian robot at 0.2 μ L final drop volume in sitting drop 96-well format using a limited in-house designed matrix of crystallization conditions was then used to tackle conditions giving crystals of Hsp90 suitable for X-ray crystallography. Good-looking monocrystals were grown using this setup in 1.0–1.4 M sodium citrate and were extracted from the low volume drops, cryo-protected in mother liquor with 20% glycerol, and flash-frozen for in-house and synchrotron data collection. In-house data collection was performed on a Nonius rotating anode generator with Osmic confocal blue optics and a MAR345 imaging plate detector. Diffraction data were processed with MOSFLM and CCP4.²⁴ The structures were solved using molecular replacement technique with coordinates of Hsp90 available in the Protein Data Bank (pdb code: 1YER). The structures were refined using either the CNX²⁵ or AUTOBUSTER²⁶ program packages, ligands were placed manually, and manual rebuilds made in COOT.²⁷ Final validation checks were performed using MOLPROBITY,²⁸ prior to deposition of coordinates and structure factors into the Protein Data Bank.²⁹ Data set statistics of all crystal structures are given in Table 4.

Noncovalent nanoESI-MS Experiments with Compounds (1) (2) and Hsp90 (18–223). Prior to mass spectrometry experiments, the protein was desalted against 100 mM ammonium acetate buffer, pH 6.8 (adjusted with ammonia) using PD10 column (Millipore), concentrated by centrifugation using a 5 kDa cut off membrane (Amicon Ultrafree, Millipore), and then stored at 4 °C. Solutions of inhibitors were stocked in DMSO at a concentration of 1 mM. Noncovalent mass experiments were carried out on an electrospray time-of-flight mass spectrometer (Micro QTOF, Waters, Manchester, UK) equipped with an automated chip-based nanoelectrospray source (Nanomate, Advion Biosciences, Ithaca, NY) operating in the positive ion mode. External calibration was performed using a solution of cesium iodide concentrated at 0.25 mg/mL that was diluted in a 1:1 ratio of 2-propanol/water. Protein–inhibitor complexes were prepared by mixing of the protein diluted to 10 μ M in 10 mM ammonium acetate and \sim 10–20 μ M DMSO solution of inhibitor (maximum of complex formed without multiple adducts), final buffer containing \sim 2% DMSO. After a short incubation time at room

temperature, 5 μ L of samples were infused through the nozzle of the chip. All spectra were recorded over the mass range m/z 200–5000 Da applied on the same cone voltage (35 V). Data analysis was performed with Masslynx 4.0 (Waters, Manchester, UK).

Human Full Length Hsp90 β SPR Binding Assay. SPR experiments were performed on a BIACORE SS1 instrument at 25 °C on CM5 sensorchips. Human Hsp90 was immobilized onto carboxymethyl 5' dextran surface (CM5 sensor chip) by standard amine coupling chemistry. The carboxymethyl dextran surface was activated with a 7-min injection of a 1:1 ratio of 0.4 M 1-ethyl-3-(3-dimethylaminopropyl) carbodiimide hydrochloride (EDC)/0.1 M *N*-hydroxy succinimide (NHS). Human Full Length Hsp90 was coupled to the surface with a 30 min injection of protein diluted at 230 μ g/mL in 10 mM sodium acetate (pH 5.5). Remaining activated groups were blocked with a 7 min injection of 1 M ethanolamine (pH 8.5). HBS-N (10 mM HEPES, 0.15 M NaCl, 3 mM EDTA, pH 7.4) was used as the running buffer during the immobilization process. About 9000 resonance units (RU) of protein were captured on the CM5 sensor chip.

The running buffer used during the binding assay was 50 mM Hepes pH 7.5, 150 mM KCl, 5 mM MgCl₂, and 2% DMSO. Small molecules were diluted in running buffer to concentrations of 750 or 350 nM and then serially 2-fold diluted in running buffer up to 23 nM. Compounds were injected from lowest to highest concentrations at a flow rate of 30 μ L/min for 1 min, and dissociation was monitored for an additional 3 min. Surface regeneration was not used. To subtract background noise from each data set, all samples were also run over an unmodified reference surface, and injections of running buffer were performed throughout every experiment ("double referencing"). A DMSO calibration curve was used to correct the effect of DMSO on the binding signal. Up to six data sets were fitted to a simple 1:1 interaction with mass transfer model. Association (k_a), dissociation (k_d) rate constants, equilibrium constant (K_d), and maximum binding (R_{max}) were determined using the Biacore SS1 evaluation software version 1.2.1. Because there is no regeneration during the compound injection series, bound analyte can accumulate on the receptor, thereby decreasing its binding capacity. Therefore, all binding responses were globally fitted with a 1:1 interaction model with a mass transport term that used a different maximum binding capacity (R_{max}) for each analyte injection.

Yeast Hsp82 ATPase Assay. ATPase activity of yeast Hsp82 was measured in a coupled system involving pyruvate kinase (PK) (Sigma), lactate dehydrogenase (LDH) (Roche), phosphoenolpyruvate (PEP), and NADH by measuring the decrease in absorbance at 340 nm. Yeast enzyme was preferred to human Hsp90 because its catalytic constant was 10 times better. Reactions were followed in 96-well, flat bottom, half volume, clear plates in a 100 μ L reaction volume, consisting of 100 mM Hepes-NaOH pH 7.5, 5 mM MgCl₂, 1 mM DTT, 150 mM KCl, 3% DMSO, 0.3 mM NADH, 2.5 mM PEP, 250 μ M ATP, 15 U/mL PK and LDH, and 1 μ M Hsp82 at 37 °C for 60 min. Compounds 1–8 were assayed over a 3-fold dilution series to determine IC₅₀, the inhibitor concentration that is required to achieve 50% inhibition of the enzyme activity, calculated by nonlinear least-squares regression.

Human Hsp90 Fluorescence Polarization Binding Assay. K_d of compound 8 and of 17-AAG were determined in a fluorescence polarization assay performed in a 20 mM Hepes–NaOH buffer, pH 7.15, 5 mM MgCl₂, 2 mM DTT, 50 mM KCl, and 3% DMSO in 96-well, half volume, nonbinding surface, black plates in a 100 μ L reaction volume. Then 10 nM of fluorescent-labeled geldanamycin³⁰ was used in all experiments. After overnight incubation at room temperature, the fluorescence polarization was measured at 485 nm (excitation) and 535 nm (emission). K_d of GA-FITC was first determined using Hsp90 concentrations ranging from 2.5 to 1280 nM. Competitive binding of GA-FITC was then performed using 20 nM protein and 20 concentrations of compound 8 ranging from 0.67 to 238 nM or of 17-AAG ranging from 1 to 2564 nM. Calculations were done according to Roerhl et al.³¹

Table 4. X-ray Data Collection, Statistics, and PDB Codes for the Structures of Hsp90 Bound to Compounds 1–8

compound									
1	2	1 + 2	3	4	5	6	7	8	
Data Collection									
space group	I222	I222	I222	I222	I222	I222	I222	I222	I222
cell (A ; $a = \beta = \gamma = 90^\circ$)	65.7 89.1 100.1	66.4 90.8 98.7	66.6 99.1 90.9	66.4 90.6 98.7	66.4 90.7 98.6	66.4 90.4 98.5	66.5 90.9 98.8	66.6 90.8 98.8	66.6 90.6 99.1
location of data collection	in-house	in-house	ESRF	ESRF	in-house	in-house	in-house	in-house	in-house
resolution (\AA)	1.61	1.83	1.74	1.32	1.93	1.67	1.43	1.46	1.67
no. unique reflections	38324	26359	30793	67326	21459	34725	51677	50264	35143
completeness (%)	99.9 (99.5)	99.6 (97.5)	98.6 (90.9)	95.2 (77.0)	94.8 (94.8)	99.5 (97.2)	94.1 (91.7)	96.2 (91.4)	96.3 (91.2)
average multiplicity	6.8	6.7	3.5	3.8	4.0	5.6	4.0	3.9	3.4
R_{merge} (R_{merge} last resolution shell) (%)	6.0 (49.4)	3.9 (20.9)	7.1 (38.4)	3.5 (27.5)	9.9 (39.0)	4.4 (16.9)	3.4 (17.8)	7.5 (42.4)	9.1 (41.7)
Refinement									
R_{cryst}	18.7	17.5	18.3	18.6	19.9	18.1	16.8	23.2	25.8
R_{free}	21.0	19.9	21.1	19.5	24.1	21.0	18.5	25.2	23.9
rmsd bond lengths (\AA)	0.01	0.01	0.01	0.01	0.01	0.01	0.01	0.005	0.005
rmsd bond angles (deg)	1.03	1.02	1.01	1.10	1.10	1.04	1.11	1.23	1.19
average B-factor protein (\AA^2)	18.7	18.7	22.1	13.6	18.7	15.9	12.5	16.2	17.5
average B-factor ligand (\AA^2)	12.8	9.5	15.0	8.7	12.4	10.0	11.5	11.7	12.5
average B-factor solvent (\AA^2)	41.0	31.8	38.3	27.0	30.9	28.4	26.9	27.9	29.3
PDB code	2yiw	2yix	2yk2	2yk9	2ykb	2ykc	2yke	2yjk	2yki

Downregulation of HER2 in Human SKBr3 cells. Mammary adenocarcinoma cells SKBr3, from American Type Culture Collection (ATCC) (HBT-30), which overexpress HER2 receptor tyrosine kinase, were grown in McCoy's 5A culture medium, supplemented with 10% fetal bovine serum and 1% L-glutamine. Cells (~125000 per well) were cultured at 37 °C in 12-well plates, under 1 mL volume of complete medium. Twenty-four h after the addition of compounds, cells were trypsinized, washed with PBS (phosphate buffered saline), and further incubated with 100 ng anti-HER2 antibody coupled to Phycoerythrin (BD 340552) for 30 min at 4 °C in the dark. Fluorescence was measured by fluorescence activated cell sorter (FACS) using Calibur apparatus (Becton-Dickinson) due to the expression of HER2 receptor on cell surface. The inhibition percentage of Her-2 inhibition related to compound concentration was fitted by nonlinear regression (XLfit, eq 205) and thus provided IC₅₀ values of compounds.

Evaluation of Compound 8 in P388 Murine Leukemia Model. Eight-week-old female B6D2F1 mice (Charles River, St. Germain sur l'Arbresle, France) were maintained with food and water *ad libitum*, and housed at 22 ± 2 °C for 10 days accommodation before use. B6D2F1 mice were intraperitoneally inoculated with 10⁶ P388 murine leukemia tumor cells in suspension in phosphate buffer (Dubelco's), 0.2 mL per mouse. Animals were then treated either with compound 8 at 6.2 mg/kg *iv* twice daily from day 1 to day 4 on one group (49.6 mg/kg total dose: highest nontoxic dose (HNTD) formulated in 7.5% PS80, HCl 1N pH = 3 in glucose isotonic solution) or with 17-AAG geldanamycin derivative administrated *ip* 80 mg/kg (320 mg/kg total dose: HNTD formulated in 5% DMSO, 5% PS80 in glucose isotonic solution). Mice were monitored daily for changes in body weight. Overall survival (defined as the percentage of increase in life span (%ILS) compared to control group) was used as readout following Kaplan–Meier method with ILS = [(MDD_{treated} – MDD_{control}) × 100]/MDD_{control} (MDD = median day of death). An ILS above 25% was considered to demonstrate a relevant antitumoral effect for the tested therapy. Statistical significance was determined using Newman–Keuls test after one way analysis of variance on rank transformation; *p* value <0.05 were considered to be significant.

Accession Codes

2ywjw; 2yjjx; 2yk2; 2yk9; 2ykb; 2ykc; 2yke; 2yjk; 2yki

AUTHOR INFORMATION

Corresponding Author

*Phone: (33) 1 58 93 38 32. E-mail: Herve.Minoux@sanofi.com.

ABBREVIATIONS USED

Hsp90, heat shock protein 90; LTS, low throughput screen; SBDD, structure-based drug design; DMSO, dimethyl sulfoxide; MW, molecular weight

REFERENCES

- (1) (a) Jolly, C.; Morimoto, R. I. Role of the heat shock response and molecular chaperones in oncogenesis and cell death. *J. Natl. Cancer Inst.* **2000**, *92*, 1564–1572. (b) Smith, D. F.; Whitesell, L.; Katsanis, E. Molecular chaperones: biology and prospects for pharmacological intervention. *Pharmacol. Rev.* **1998**, *50*, 493–513. (c) Smith, D. F. Chaperones in signal transduction. In *Molecular Chaperones in the Cell*; Lund, P., Ed.; Oxford University Press: Oxford, 2001; pp 165–178.
- (2) Hanahan, D.; Weinberg, R. A. The hallmark of cancer. *Cell* **2000**, *100*, 57–70.
- (3) Whitesell, L.; Lundquist, S. L. Hsp90 and the chaperoning of cancer. *Nature Rev. Cancer* **2005**, *5*, 761–772.
- (4) Workman, P.; Burrows, F.; Neckers, L.; Rosen, N. Drugging the cancer chaperone Hsp90: combinatorial therapeutic exploitation of

oncogene addiction and tumor stress. *Ann. N. Y. Acad. Sci.* **2007**, *111*, 202–216.

(5) For extensive reviews see: (a) Janin, Y. L. Heat shock protein 90 inhibitors. A text book example of medicinal chemistry. *J. Med. Chem.* **2005**, *48*, 7503–7512. (b) Janin, Y. L. ATPase inhibitors of Hsp90, second season. *Drug Discovery Today* **2010**, *15*, 342–353. (c) Patel, H. J.; Modi, S.; Chiosis, G.; Taldone, T. Advances in the discovery and development of heat-shock protein 90 inhibitors for cancer treatment. *Expert. Opin. Drug Discovery* **2011**, *6*, 559–587. (d) Kim, Y. S.; Alarcon, S. V.; Lee, S.; Lee, M.-J.; Giaccone, G.; Neckers, L.; Trepel, J. B. Update on Hsp90 inhibitors in clinical trial. *Curr. Top. Med. Chem.* **2009**, *9*, 1479–1492.

(6) Trepel, J.; Mollapour, M.; Giaccone, G.; Neckers, L. Targeting the dynamic Hsp90 complex in cancer. *Nature Rev. Cancer* **2010**, *10*, 537–549.

(7) Biamonte, M. A.; van de Water, R.; Arndt, J. W.; Scannevin, R. H.; Perret, D.; Lee, W. C. Heat shock protein 90: inhibitors in clinical trials. *J. Med. Chem.* **2010**, *53*, 3–17.

(8) Loo, J. A. Studying noncovalent protein complexes by electrospray ionisation mass spectrometry. *Mass Spectrom. Rev.* **1997**, *16*, 1–23.

(9) Potier, N.; Barth, P.; Trisch, D.; Biellmann, J.-F.; van Dorsselaer, A. Study of non-covalent enzyme–inhibitor complexes of aldose reductase by electrospray mass spectrometry. *Eur. J. Biochem.* **1997**, *243*, 274–282.

(10) (a) Gourves, J. P.; Couthon, H.; Sturtz, G. Synthesis of 3,4-dihydro-2H-pyrido[1,2-*b*]isoindol-1-one and 3,4-dihydro-2H-pyrido[1,2-*b*]pyrrolidin-1-one functionalized at the C-6 position by an intramolecular Horner–Wadsworth–Emmons reaction. *Eur. J. Org. Chem.* **1999**, *1999*, 3489–3493. (b) Deok-Chan, H.; Chang-Soo, Y.; Eunsun, Y. Reductive cyclization of *N*-iodoalkyl cyclic imides to nitrogen-fused polycyclic amides induced by samarium diiodide. *Tetrahedron Lett.* **1996**, *37*, 2577–2580. (c) Earl, R. A.; Volhardt, P. C. On the synthetic utility of thermally generated imines: the retro-ene imino Diels–Alder reaction. *Heterocycles* **1982**, *19*, 265–271. (d) Mazzochi, P. H.; Klingler, L.; Edwards, M.; Wilson, P.; Shook, D. Intra- and intermolecular Paterno–Büchi reactions on phthalimides. Isolation of the oxetane. *Tetrahedron Lett.* **1983**, *24*, 143–146. (e) Marion, F.; Courillon, C.; Malacria, M. Radical cyclization cascade involving ynamides: an original access to nitrogen-containing heterocycles. *Org. Lett.* **2003**, *5*, 5095–5097.

(11) Bacque, E.; Benard, D.; Bertin, L.; Carrez, C.; Mailliet, P.; Vallee, F. New isoindole derivatives, compositions containing same, preparation thereof and pharmaceuticals uses thereof in particular as inhibitors of chaperone protein HSP90 activities. Patent WO 2006 108948, 2006

(12) Mailliet, P.; Bertin, L.; Guyon, T.; Thompson, F.; Ruxer, J.-M.; Pilorge, F.; Benard, D.; Minoux, H.; Carrez, C.; Goulaouic, H. Novel fluorene derivatives, composition containing said derivatives and the use thereof. Patent WO 2006 123061, 2006.

(13) Zhou, V.; Han, S.; Brinker, A.; Klock, H.; Caldwell, J.; Gu, X.-J. A time-resolved fluorescence resonance energy transfer-based HTS assay and a surface plasmon resonance-based binding assay for heat shock protein 90 inhibitors. *Anal. Biochem.* **2004**, *331*, 349–357.

(14) Hopkins, A. L.; Groom, C. R.; Alex, A. Ligand efficiency: a useful metric for lead selection. *Drug Discovery Today* **2004**, *9*, 430–431.

(15) Drysdale, M. J.; Dymock, B. W.; Finch, H.; Webb, P.; McDonald, E.; James, K. E.; Cheung, K. M.; Mathews, T. P. Preparation of Isoxazoles as Inhibitors of Heat Shock Proteins. Patent WO 2004 72051, 2005.

(16) Cox, P. J.; Majid, T. N.; Lai, J. Y. Q.; Morley, A.; Amendola, S.; Deprets, S. D.; Edlin, C.; Gardner, C. J.; Kominos, D.; Pedgrift, B. L.; Halley, F.; Gillespie, T. A.; Edwards, M.; Clerc, F. F.; Nemecek, C.; Houille, O.; Damour, D.; Bouchard, H.; Bezaud, D.; Carrez, C. Azaindoles. Patent WO 2003 000688, 2003.

(17) Lipinski, C. A.; Lombardo, F.; Dominy, B. W.; Feeney, P. J. Experimental and computational approaches to estimate solubility and permeability in drug discovery and development settings. *Adv. Drug Delivery Rev.* **1997**, *23*, 3–25.

(18) (a) Jones, G.; Willett, P.; Glen, R. C. Molecular Recognition of Receptor Sites Using a Genetic Algorithm with a Description of

Desolvation. *J. Mol. Biol.* **1995**, *245*, 43–53. (b) Jones, G.; Willett, P.; Glen, R. C.; Leach, A. R.; Taylor, R. Development and Validation of a Genetic Algorithm for Flexible Docking. *J. Mol. Biol.* **1997**, *267*, 727–748.

(19) *Maestro*, version 8.0; Schrödinger, LLC, New York, NY, 2007.

(20) (a) *MacroModel*, version 9.5; Schrödinger, LLC, New York, NY, 2007. (b) Jorgensen, W. L.; Tirado-Rives, J. The OPLS Force Field for Proteins. Energy Minimizations for Crystals of Cyclic Peptides and Crambin. *J. Am. Chem. Soc.* **1988**, *110*, 1657–1666. (c) Jorgensen, W. L.; Maxwell, D. S.; Tirado-Rives, J. Development and Testing of the OPLS All-Atom Force Field on Conformational Energetics and Properties of Organic Liquids. *J. Am. Chem. Soc.* **1996**, *118*, 11225–11236.

(21) Allen, F. H. The Cambridge Structural Database: a quarter of a million crystal structures and rising. *Acta Crystallogr., Sect. B: Struct. Sci.* **2002**, *58*, 380–388.

(22) Bruno, I. J.; Cole, J. C.; Edgington, P. R.; Kessler, M.; Macrae, C. F.; McCabe, P.; Pearson, J.; Taylor, R. New software for searching the Cambridge Structural Database and visualising crystal structures. *Acta Crystallogr., Sect. B: Struct. Sci.* **2002**, *58*, 389–397.

(23) Prodromou, C.; Piper, P. W.; Pearl, L. H. Expression and crystallization of the yeast Hsp82 chaperone, and preliminary X-ray diffraction studies of the amino-terminal domain. *Proteins* **1996**, *25*, 517–522.

(24) Collaborative Computational Project, No. 4. The CCP4 suite: programs for protein crystallography. *Acta Crystallogr., Sect. D: Biol. Crystallogr.* **1994**, *50*, 760–763.

(25) Brunger, A. T.; Adams, P. D.; Clore, G. M.; DeLano, W. L.; Gros, P.; Grosse-Kunstleve, R. W.; Jiang, J. S.; Kuszewsky, J.; Nilges, M.; Pannu, N. S.; Read, R. J.; Rice, L. M.; Simonson, T.; Warren, G. L. Crystallography and NMR system; a new software suite for macromolecular structure determination. *Acta Crystallogr., Sect. D: Biol. Crystallogr.* **1998**, *54*, 905–921.

(26) Bricogne, G. Direct phase determination by entropy maximization and likelihood ranking: status report and perspectives. *Acta Crystallogr., Sect. D: Biol. Crystallogr.* **1993**, *49*, 37–60.

(27) Emsley, P.; Cowtan, K. Coot: model-building tools for molecular graphics. *Acta Crystallogr., Sect. D: Biol. Crystallogr.* **2004**, *60*, 2126–2132.

(28) Chen, V. B.; Arendall, W. B., III; Headd, J. J.; Keedy, D. A.; Immormino, R. M.; Kapral, G. J.; Murray, L. W.; Richardson, J. S.; Richardson, D. C. MolProbity: all-atom structure validation for macromolecular crystallography. *Acta Crystallogr., Sect. D: Biol. Crystallogr.* **2010**, *66*, 12–21.

(29) Berman, H. M.; Westbrook, J.; Feng, Z.; Gilliland, G.; Bhat, T. N.; Weissig, H.; Shindyalov, I. N.; Bourne, P. E. The Protein Data Bank. *Nucleic Acids Res.* **2000**, *28*, 235–242.

(30) Llauger-Bufi, L.; Felts, S. J.; Huezo, H.; Rosen, N.; Chiosis, G. Synthesis of Novel fluorescent probes for the molecular chaperone Hsp90. *Bioorg. Med. Chem. Lett.* **2003**, *13*, 3975–3978.

(31) Roehrl, M. H. A.; Wang, J. Y.; Wagner, G. A general framework for development and data analysis of competitive high-throughput screens for small-molecule inhibitors of protein–protein interactions by fluorescence polarization. *Biochemistry* **2004**, *43*, 16056–16066.